

(A New Proposal to Jefferson Lab PAC23)

# Polarization transfer in Wide Angle Compton Scattering

J. P. Chen, E. Chudakov, C. DeJager, R. Feuerbach, J. Gomez, O. Hansen,  
D. W. Higinbotham, M. Jones, J. LeRose, R. Michaels, S. Nanda,  
B. Reitz, A. Saha, B. Wojtsekhowski (spokesperson and contact person)  
*Thomas Jefferson National Accelerator Facility, Newport News, VA 23606*

A. Danagouliau, A.M. Nathan (spokesperson), M. Roedelbronn  
*University of Illinois, Champaign-Urbana, IL 61801*

V. Kubarovsky<sup>†</sup>, J. Napolitano, P. Stoler  
*Rensselaer Polytechnic Institute, Troy, NY 12180-3590*

K. Egiyan, V. Mamyan, A. Shahinyan, H. Voskanyan  
*Yerevan Physics Institute, Yerevan, Armenia*

F. Cusanno, F. Garibaldi, S. Frullani, G. M. Urciuoli, M. Iodice  
*INFN, Rome, Italy*

R. De Leo, L. La Gamba      D. Nikolenko, I. Rachek, Yu. Shestakov  
*INFN, Bari, Italy      Budker Institute, Novosibirsk, Russia*

Seonho Choi, F. Butaru, Z.-E. Meziani, K. Slifer, P. Solvignon, H. Yao  
*Temple University, Philadelphia, PA 19122*

P. Bosted  
*University of Massachusetts*

J. Annand, A. Borissov, D. Hamilton, D. Ireland, D. Protopopescu,  
G. Rosner, D. Watts  
*University of Glasgow, Glasgow, Scotland*

P. Markowitz  
*Florida International University, Miami, FL 33199*

G. Chang, J. J. Kelly  
*University of Maryland, College Park, MD 20792*

M. Khandaker, V. Punjabi  
*Norfolk State University, Norfolk, VA 23504*

B. Crowe, B. Vlahovic  
*North Carolina Central University, Durham, NC 03824*

F. Benmokhtar, C. Glashausser, R. Gilman, X. Jiang,  
G. Kumbartzki, K. McCormick, R. Ransome, J. Yuan  
*Rutgers, The State University of New Jersey, Piscataway, NJ 08854*

J. M. Laget, F. Sabatie  
*CEA Saclay, Gif-sur-Yvette, France*

E. Piasetzky, G. Ron  
*Tel Aviv University, Israel*

C. Perdrisat, L. Pentchev  
*College of William and Mary, Williamsburg, VA 23185*

C. Hyde-Wright, A. Radyushkin,  
*Old Dominion University*

A. Vasiliev  
*IHEP, Protvino, Russia*

O. Gayou  
*Massachusetts Institute of Technology*

V. Nelyubin  
*St-Petersburg Institute Nuclear Physics, Russia*

D. Margaziotis  
*California State University Los Angeles, Los Angeles, CA 90032*

<sup>†</sup> on leave from *IHEP, Protvino, Russia*

December 3, 2002

### Abstract

An experiment is proposed to measure the components of the recoil proton polarization in Real Compton Scattering (RCS) with longitudinally polarized incident photons. Measurements are proposed at  $s = 7 \text{ (GeV}/c)^2$  for four values of the  $\theta_\gamma^{cm} = 60^\circ, 100^\circ, 140^\circ$ , and  $160^\circ$ .

The recent JLab RCS experiment, E99-114, not only demonstrated the feasibility of the experimental technique but also produced a remarkable result. Namely, at  $s = 7 \text{ (GeV}/c)^2$  and  $\theta_\gamma^{cm} = 120^\circ$ , the longitudinal polarization is in agreement with the handbag description of the process in which the photons interact with a single quark and inconsistent with a pQCD mechanism which involves three active quarks. It is essential to have additional measurements over a broader kinematic range for complete experimental verification of the handbag mechanism. Besides testing the reaction mechanism, the measurements will also allow access to the axial and tensor form factors of the proton,  $R_A$  and  $R_T$ , respectively, which are moments of particular Generalized Parton Distributions.

The experiment utilizes an untagged bremsstrahlung photon beam and the standard Hall A cryogenic target. The scattered photon is detected in the BigCal photon spectrometer, currently under construction by the GEP-III collaboration. The coincident recoil proton is detected in the Hall A magnetic spectrometer HRS-L, and its polarization components are measured in the existing Focal Plane Polarimeter. One kinematic point will require a Hall A septum magnet. With 312 hours of beam time, each of the three polarization observables,  $K_{LL}$ ,  $K_{LT}$ , and  $P_N$ , will be measured to a statistical accuracy of better than  $\pm 0.1$  at each kinematic point.

Such a measurement would significantly increase our experimental confidence in the handbag reaction mechanism which is expected to play a major role in exclusive reactions in the JLab energy range.

# 1 Introduction

Compton scattering in the hard scattering limit is a potentially powerful probe of the short-distance structure of the nucleon. It is a natural complement to other exclusive reactions, such as high  $Q^2$  elastic electron scattering and high-energy meson photoproduction, where the common feature is a hard energy scale. For Real Compton Scattering (RCS), the hard scale is achieved when  $s$ ,  $-t$ , and  $-u$  are all large compared to the proton mass, or equivalently, when the transverse momentum transfer  $p_\perp$  is large. Under such conditions one expects the transition amplitude to factorize into the convolution of a perturbative hard scattering amplitude, which involves the coupling of the external photons to the active quarks, with an overlap of initial and final soft (nonperturbative) wave functions, which describes the coupling of the active quarks to the proton. Schematically this can be written

$$T_{if}(s, t) = \Psi_f \otimes K(s, t) \otimes \Psi_i, \quad (1)$$

where  $K(s, t)$  is the perturbative hard scattering amplitude, and the  $\Psi$ 's are the soft wave functions. Different factorization schemes have been applied to RCS in recent years and these can be distinguished by the number of active constituents participating in the hard scattering subprocess. The perturbative QCD (pQCD) mechanism [1, 2, 3, 4] involves three active constituents, while the handbag mechanism [5, 6, 7] involves only one. In any given kinematic regime, both mechanisms will contribute, in principle, to the scattering amplitude. At “sufficiently high” energy, the pQCD mechanism is expected to dominate, but it is not known how high is sufficiently high or the manner in which the transition to the purely pQCD mechanism emerges. At sufficiently low energy (e.g., in the resonance region), RCS and other exclusive reactions are dominated by purely soft physics, and the amplitude does not factorize into hard and soft processes. At high energy but small  $-t$  or  $-u$ , soft physics also dominates through Regge exchanges [8]. The nature of the transition from purely soft to the factorization regime is also not well known.

Quite aside from the reaction mechanism, it is of interest to ask what RCS can teach us about the nonperturbative structure of the proton and to relate it to that revealed in other reactions. There has been much theoretical progress in recent years in providing a unified description of inclusive and exclusive reactions in the hard scattering regime [5, 6, 7]. This is based on the concept of Generalized Parton Distributions (GPD's), which are superstructure of the nucleon from which can be derived the normal parton distribution functions (PDF's), elastic electron scattering form factors, and other quantities that have yet to be measured, including new form factors accessible only through Compton scattering.

With this backdrop, experiment E99-114 [9] was proposed to study the RCS reaction. After a 2.5-year period of construction and testing of a new photon detector, the data taking was completed early in 2002. The primary focus was the measurement of precise spin-averaged cross sections over the kinematic regime of  $5 \leq s \leq 11$  (GeV/c)<sup>2</sup> and  $1.5 \leq -t \leq 6.5$  (GeV/c)<sup>2</sup>. In addition, a measurement was made at a single kinematic point of the polarization transfer to the recoil proton using longitudinally polarized incident photons.

Although the data analysis is still in progress, the measurement of the polarization has already produced a remarkable result, which is shown in Fig. 1 and which will be discussed in more detail in the next section of this proposal. Namely, the longitudinal polarization transfer is consistent with the handbag prediction and completely inconsistent with predictions based on pQCD. This give very strong credence to the notion that the photons interact with a single quark. Indeed, the longitudinal polarization is nearly as large as that expected for scattering from a free quark. However, we emphasize that this is a measurement at a *single kinematic point*, and it is essential to verify the result with measurements over a broader kinematic range.

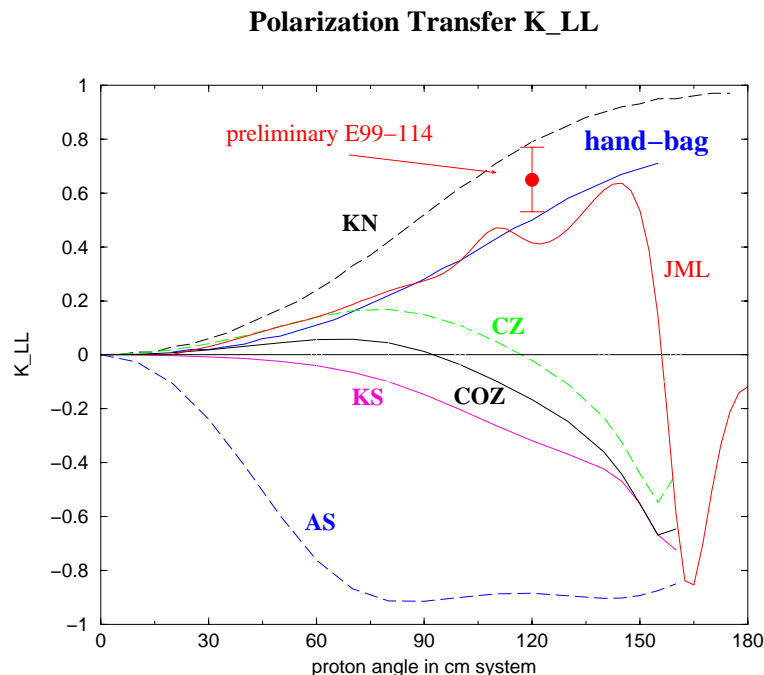


Figure 1: Longitudinal polarization transfer in the RCS process at an incident energy of 3.23 GeV. The labels on the curves are KN for the asymmetry in the hard subprocess; handbag for calculations in handbag approach [7]; the pQCD calculations [4] with AS for asymptotic distribution amplitudes, CZ for Chernyak-Zhitnitsky, COZ for Chernyak-Ogloblin-Zhitnitsky, and KS for King-Sachrajda; and JML for calculations using a Regge exchange model.

We therefore propose new measurements of polarization observables in Compton scattering at an incident energy of 3.23 GeV at four different scattering angles. The proposal is organized as follows. In Section 2 we present our physics motivation and summarize the physics goals of the proposed experiment. In Section 3 we describe the experimental approach and both the standard and the specialized equipment. In subsequent sections, we present our proposed measurements (Sec. 4), our expected results and beam time request (Sec. 5), and the technical considerations related to the equipment and the experiment schedule (Sec. 6). The proposal is summarized in Section 7.

## 2 Physics Motivation

### 2.1 Overview

In view of the remarks in the Introduction, we consider several interesting questions that motivates us to explore further the measurement of polarization observables in RCS at JLab:

1. Is it indeed true that the RCS reaction proceeds through the interaction of the photons with a single quark?
2. What information can be learned about the structure of the proton from new measurements of the polarization observables and how is this structure related to that measured in other exclusive reaction?
3. At what kinematic scale is factorization into hard and soft process valid?

In order to present a framework for addressing these issue, we next present discussions of three reaction mechanisms: the pQCD, handbag, and Regge exchange mechanisms.

### 2.2 pQCD Mechanism

The traditional framework for the interpretation of hard exclusive reactions has been perturbative QCD (pQCD) [10]. This is based in part on the observation that the onset of scaling in Deep Inelastic Scattering (DIS) occurs at the relative low scale of  $Q^2 \sim 1\text{--}2$  (GeV/c)<sup>2</sup>, thereby giving rise to expectations that pQCD might also be applicable to the exclusive processes in the range of a few (GeV/c)<sup>2</sup>. The pQCD approach to RCS [1, 2, 3, 4] is shown in Fig. 2.2, where it is seen that the three valence quarks are active participants in the hard subprocess, which is mediated by the exchange of two hard gluons. The soft physics is contained in the so-called valence quark distribution amplitudes. The pQCD mechanism leads naturally to the so-called constituent counting rules for exclusive processes:

$$\frac{d\sigma}{dt} = \frac{f(\theta_{cm})}{s^n}, \quad (2)$$

where  $n$  is related to the number of active constituents in the reaction [11, 12]. Indeed, the observation that many exclusive reactions, such as elastic electron scatter, pion photoproduction, and RCS, approximately obey Eq.2 has led to the belief that the pQCD mechanism dominates at experimentally accessible energies. There seems to be little theoretical disagreement that the pQCD mechanism dominates at sufficiently high energies [13]; however, there is no consensus on how high is “sufficiently high.” Indeed, despite the observed scaling, absolute cross sections calculated using the pQCD framework are very often low compared to existing experimental data, sometimes by more than an order of magnitude. Moreover, several recent JLab experiments that measure polarization observables also disagree with the predictions of pQCD. In the  $G_E^p$  experiment [14, 15] the slow falloff of the Pauli form factor  $F_2(Q^2)$  up to  $Q^2$  of 5.5 (GeV/c)<sup>2</sup> provides direct evidence that hadron helicity is not

conserved, contrary to predictions of pQCD. Similar findings were made in the  $\pi^0$  photo-production experiment [16], where both the non-zero transverse and normal components of polarization of the recoil proton are indicative of hadron helicity-flip, which is again contrary to the predictions of pQCD. Finally, in the recently completed RCS experiment, E99-114, the preliminary analysis of the longitudinal polarization transfer  $K_{LL}$  (which will be defined precisely below) shows a value which is large and positive, contrary to the pQCD prediction which is negative. For all these reasons, we conclude the pQCD is not the correct mechanism for interpreting exclusive reactions at accessible energies and instead seek a description in terms of the handbag mechanism.

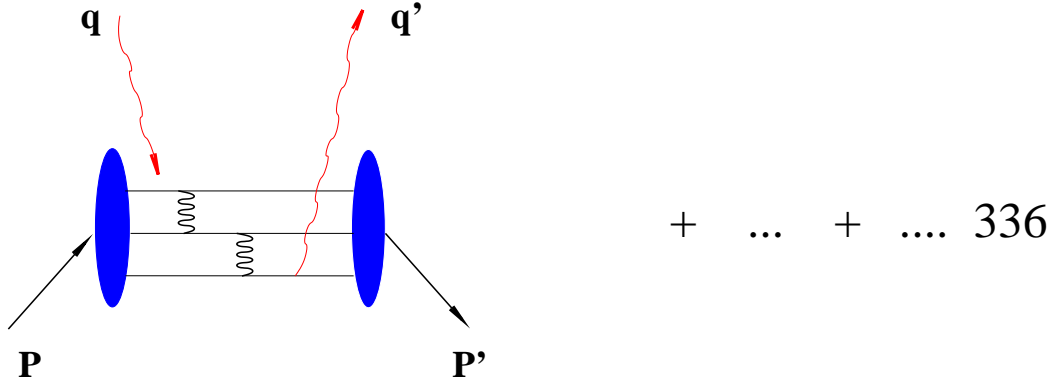


Figure 2: Two gluon exchange pQCD diagram for RCS.

### 2.3 Handbag Mechanism

The handbag mechanism offers new possibilities for the interpretation of hard exclusive reactions. For example, it provides the framework for the interpretation of so-called deep exclusive reactions, which are reactions initiated by a high- $Q^2$  virtual photon. The application of the formalism to RCS (see Fig. 3) was initially worked out to leading order (LO) by Radyushkin [5] and subsequently by Diehl [6]. More recently next-to-leading-order (NLO) contributions have been worked out by Huang and Kroll [7]. The corresponding diagram for elastic electron scattering is similar to Fig. 3, except that there is only one external virtual photon rather than two real photons. In the handbag approach, the hard physics is contained in the scattering from a single active quark and is calculable using pQCD and QED: it is just Compton scattering from a structureless spin-1/2 particle. The soft physics is contained in the wave function describing how the active quark couples to the proton. This coupling is described in terms of GPD's. The GPD's have been the subject of intense experimental and theoretical activity in recent years [17, 18]. They represent “superstructures” of the proton, from which are derived other measurable structure functions, such as parton distribution functions (PDF) and form factors. To NLO, only three of the four GPD's contribute to the

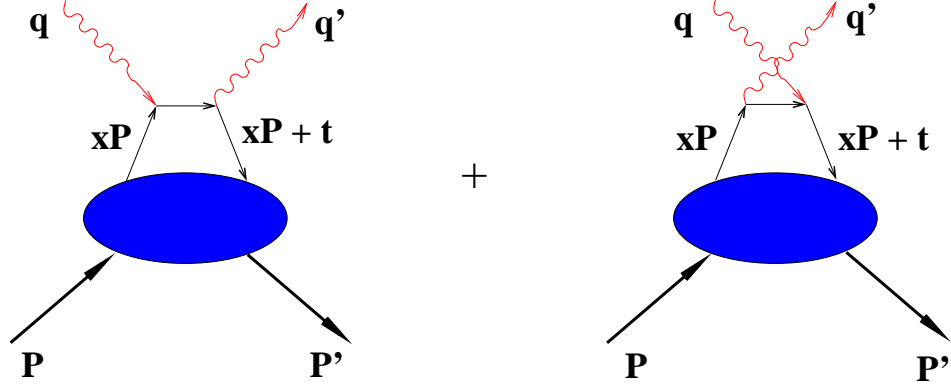


Figure 3: The handbag diagram for RCS.

RCS process:  $H(x, \xi = 0, t)$ ,  $\hat{H}(x, \xi = 0, t)$ , and  $E(x, \xi = 0, t)$ . Since the photons are both real, the so-called skewness parameter  $\xi=0$ , reflecting the fact that the momentum absorbed by the struck quark is purely transverse. In the handbag formalism, the RCS observables are new form factors of the proton that are  $x^{-1}$ -moments of the GPD's:

$$\begin{aligned} R_V(t) &= \sum_a e_a^2 \int_{-1}^1 \frac{dx}{x} H^a(x, 0, t), \\ R_A(t) &= \sum_a e_a^2 \int_{-1}^1 \frac{dx}{x} \text{sign}(x) \hat{H}^a(x, 0, t), \\ R_T(t) &= \sum_a e_a^2 \int_{-1}^1 \frac{dx}{x} E^a(x, 0, t), \end{aligned}$$

where  $e_a$  is the charge of the active quark and the three form factors are, respectively, the vector, axial vector, and tensor form factors. The corresponding form factors for elastic electron or neutrino scattering are given by the  $x^0$ -moments of the same GPD's:

$$\begin{aligned} F_1(t) &= \sum_a e_a \int_{-1}^1 dx H^a(x, 0, t), \\ G_A(t) &= \sum_a \int_{-1}^1 dx \text{sign}(x) \hat{H}^a(x, 0, t), \\ F_2(t) &= \sum_a e_a \int_{-1}^1 dx E^a(x, 0, t), \end{aligned}$$

where the three quantities are, respectively, the Dirac, axial, and Pauli form factors. On the other hand, the  $t = 0$  limit of the GPD's produce the PDF's:

$$H^a(x, 0, 0) = q^a(x),$$



$$\begin{aligned}
\hat{H}^a(x, 0, 0) &= \Delta q^a(x) \\
E^a(x, 0, 0) &= 2 \frac{J^a(x)}{x} - q^a(x),
\end{aligned} \tag{3}$$

where  $J^a$  is the total angular momentum of quark flavor  $a$  and is not directly measurable in DIS.

In the handbag factorization scheme, the RCS helicity amplitudes are related to the form factors by

$$\begin{aligned}
M_{\mu'+, \mu+}(s, t) &= 2\pi\alpha_{em} [T_{\mu'+, \mu+}(s, t)(R_V(t) + R_A(t)) + T_{\mu'-, \mu-}(s, t)(R_V(t) - R_A(t))], \\
M_{\mu'-, \mu+}(s, t) &= 2\pi\alpha_{em} \frac{\sqrt{-t}}{m} [T_{\mu'+, \mu+}(s, t) + T_{\mu'-, \mu-}(s, t)] R_T(t),
\end{aligned}$$

where  $\mu, \mu'$  denote the helicity of the incoming and outgoing photons, respectively. The signs on  $M$  and  $T$  refer to the helicities of the proton and active quark, respectively. This structure of the helicity amplitudes leads to a simple interpretation of the RCS form factors:  $R_V \pm R_A$  is the response of the proton to the emission and reabsorption of quarks with helicity in the same/opposite direction of the proton helicity, and  $R_T$  is directly related to the proton helicity-flip amplitude [7].

These equations leads to expressions relating RCS observables to the form factors. The most important of these experimentally are the spin-averaged cross section and the recoil polarization observables. The spin-averaged cross section factorizes into a simple product of the Klein-Nishina (KN) cross section describing the hard scattering from a single quark and a sum of form factors depending only on  $t$  [5, 6]:

$$\frac{d\sigma/dt}{d\sigma_{\text{KN}}/dt} = f_V \left[ R_V^2(t) + \frac{-t}{4m^2} R_T^2(t) \right] + (1 - f_V) R_A^2(t), \tag{4}$$

For the the interesting region of large  $p_\perp$ , the kinematic factor  $f_V$  is always close to 1. Consequently the unpolarized cross sections are largely insensitive to  $R_A$ , and the left-hand-side of Eq. 4 is nearly  $s$ -independent at fixed  $t$ . The recent calculations to NLO, which take into account both photon and proton helicity-flip amplitudes, do not change this prediction in any appreciable way [7]. One of the primary goals of E99-114 was to test this relationship as well as to determine the vector form factor  $R_V$ . The longitudinal and transverse polarization transfer observables,  $K_{LL}$  and  $K_{LT}$ , respectively, are defined by

$$K_{LL} \frac{d\sigma}{dt} \equiv \frac{1}{2} \left[ \frac{d\sigma(\uparrow\downarrow)}{dt} - \frac{d\sigma(\uparrow\uparrow)}{dt} \right] \quad K_{LT} \frac{d\sigma}{dt} \equiv \frac{1}{2} \left[ \frac{d\sigma(\uparrow\rightarrow)}{dt} - \frac{d\sigma(\downarrow\rightarrow)}{dt} \right] \tag{5}$$

where the first arrow refers to the incident photon helicity and the second to the recoil proton helicity ( $\uparrow$ ) or transverse polarization ( $\rightarrow$ ). The induced polarization of the recoil proton

normal to the scattering plane,  $P_N$ , is defined by

$$P_N \frac{d\sigma}{dt} \equiv \frac{1}{2} \left[ \frac{d\sigma(\uparrow)}{dt} - \frac{d\sigma(\downarrow)}{dt} \right] \quad (6)$$

and is independent of the incident photon polarization. Here  $\uparrow$  and  $\downarrow$  denote the component of polarization up and down, respectively, with respect to the scattering plane. With definitions of two additional parameters

$$\beta = \frac{2m}{\sqrt{s}} \frac{\sqrt{-t}}{\sqrt{s} + \sqrt{-u}} \quad \kappa(t) = \frac{\sqrt{-t}}{2m} \frac{R_T(t)}{R_V(t)}, \quad (7)$$

the three polarization observables are approximately related to the form factors by the expressions [6, 7]

$$K_{LL} \approx K_{LL}^{\text{KN}} \frac{R_A(t)}{R_V(t)} \frac{1 - \beta\kappa(t)}{1 + \kappa^2(t)} \quad \frac{K_{LT}}{K_{LL}} \approx \kappa(t) \frac{1 + \beta\kappa^{-1}(t)}{1 - \beta\kappa(t)} \quad P_N \approx 0, \quad (8)$$

where  $K_{LL}^{\text{KN}}$  is the longitudinal asymmetry for a structureless Dirac particle. These formulas do not include small gluonic corrections, which are discussed in Ref. [7].

These expressions show that measurements of  $K_{LL}$  and  $K_{LT}$ , when combined with measurements of  $d\sigma/dt$  from E99-114, allow determinations of all three form factors. They also show that two very important pieces of information follow directly from the spin asymmetries:  $K_{LL}$  and  $K_{LL}/K_{LT}$ , which are directly related to the form factor ratios  $R_A/R_V$  and  $R_T/R_V$ , respectively.

From the relationships connecting RCS form factors to PDF's, Eq. 3, the ratio  $R_A/R_V$  is related to  $\Delta q^a(x)/q^s(x)$ . For RCS, the  $e_a^2$ -weighting of the quark flavors means that  $u$  quarks will dominate the reaction. Moreover, at moderate-to-high  $-t$ , the contributions to the form-factor integral are concentrated at moderate-to-high  $x$ , where the valence quarks dominate. Therefore, the  $K_{LL}$  asymmetry has direct information on  $\Delta u(x)/u(x)$  in the valence region. Obtaining this kind of information is one of the key justifying physics goals for a possible 12 GeV upgrade of JLab.

From the correspondence between RCS and electron scattering form factors, there is expected to be a close relationship between  $R_T/R_V$  and  $F_2/F_1$  [7]. The recent JLab  $G_E^p$  experiments [14, 15] have shown that  $F_2/F_1$  falls as  $1/\sqrt{-t}$  rather than as  $1/t$ , the latter being predicted by pQCD. It will be an important check on the theoretical interpretation of  $F_2/F_1$  to see if  $R_T/R_V$  behaves in a similar way. In the current context, this means that the parameter  $\kappa(t)$ , and therefore  $K_{LT}/K_{LL}$ , would be nearly independent of  $t$ . We propose to investigate this in the present experiment, up to  $-t = 5 / (\text{GeV}/c)^2$ .

Finally, we note that the quantity  $P_N$  is predicted to vanish to NLO, except for possible gluonic contributions, which involve additional (unknown) soft form factors [7]. These contributions have been estimated to contribute no more than about 0.03 to  $P_N$ . An accurate experimental determination of  $P_N$  will be helpful in obtaining better estimates of the gluonic contributions to both  $K_{LL}$  and  $K_{LT}$ .

## 2.4 Regge Exchange Mechanism

When  $s$ ,  $-t$ , and  $-u$  are not sufficiently large, then the factorization into hard and soft process may not apply, in which case neither the pQCD nor the handbag approach is valid. An alternative approach has been proposed by Laget [8] based on Vector Meson Dominance (VMD). In the VMD approach, the photon fluctuates into a vector meson, which then interacts with the target via  $t$ -channel exchange of mesons (which dominates at low  $t$  or forward angles) or  $u$ -channel exchange of baryons (which dominates at low  $u$  or backward angles). The open question is how high  $t$  or  $u$  must be in order that the VMD mechanism becomes small compared to the handbag mechanism. The VMD model has had recent successes even at moderately large  $t$ . For example the VMD model is able to account for the observed low value of the  $G_E^p$  form factor [15] at  $-t = 5.6 \text{ (GeV}/c)^2$  [19].

Real and Virtual Compton Scattering were studied in a model based on Regge trajectories and two-gluon exchange by F. Cano and J.-M. Laget [8]. The parameters of the model were “tuned” by fitting data from vector meson photonproduction [20, 21], giving rise to predictions for the cross section and spin observables in RCS involving only a single free parameter, the radiative decay constant of the  $\rho$  meson. Given the close agreement over much of the kinematic range between the handbag and VMD predictions, they point out that at presently accessible momentum transfer, the contribution to RCS from the hadronic component of the photon is not negligible (see review [22]). For example the predicted longitudinal polarization transfer (see Fig. 1)  $A_{LL}$  is positive, close to the prediction of the handbag approach at  $\theta_\gamma^{cm}$  below  $140^\circ$ , and close to the preliminary result from E99-114. However, it strongly deviates from the handbag prediction at larger angles, where the  $u$ -channel exchange of baryons becomes dominant. We propose a measurement at  $\theta_\gamma^{cm}=160^\circ$  where  $-u$  is small and the handbag mechanism is not expected to apply in order to test directly the VMD model prediction.

## 2.5 Additional Remarks

It is important to realize that the issues posed at the start of this section are not limited to the RCS reaction. Indeed, they are questions that need to be addressed by all studies of the proton using exclusive reactions in the hard scattering regime. The old paradigm for addressing these questions was the pQCD mechanism and the distribution amplitudes. It is quite likely that the new paradigm will be the handbag mechanism and GPD's. In any case, the reaction mechanism needs to be tested, not only over a wide range of kinematic variables but also over a wide range of different reactions. Of these, RCS offers the best possibility to test the mechanism free of complications from additional hadrons.

It is also important to realize that any evidence for nonzero  $K_{LT}$  and  $P_N$  is evidence for hadron helicity flip. Such evidence has already been seen in the  $G_E^p/G_M^p$  experiment, as discussed above. Independent of whether the handbag formalism is the correct one, it is quite likely that there is a very close relationship between  $K_{LT}/K_{LL}$  and  $F_2/F_1$ , and it is important to discover what that relationship is.

## 2.6 Summary of Physics Goals

We propose measurements of the spin asymmetries  $K_{LL}$ ,  $K_{LT}$ , and  $P_N$  at an incident photon energy of 3.23 GeV ( $s=6.9 \text{ (GeV}/c)^2$ ) at four different scattering angles corresponding to  $-t$  in the range 1.3 to 5.1  $(\text{GeV}/c)^2$ . The specific physics goals are as follows:

1. Provide a stringent test of the notion that the RCS reaction proceeds via the interaction of the photons with a single quark.
2. Determine the form factor ratio  $R_T/R_V$  from measurements of  $K_{LT}/K_{LL}$  and correlate these measurements with the corresponding values of  $F_2/F_1$  determined from elastic electron scattering.
3. Determine the form factor ratio  $R_A/R_V$ .
4. Measure  $P_N$  in order to aid in the further development of the theoretical framework.
5. Test the VMD predictions relative to the handbag predictions by a measurement of  $A_{LL}$  at  $\theta_\gamma^{cm}=160^\circ$ .

The overall statistical precision with which we will address these physics goals will be discussed in Sec. 5.

### 3 Experimental Setup

The proposed experiment will study the scattering of polarized photons from a liquid hydrogen target, as illustrated in Fig. 4. The scattered photon will be detected in the BigCal calorimeter installed at a distance to match the acceptance of the HRS-left, which will be used to detect the recoiling proton.

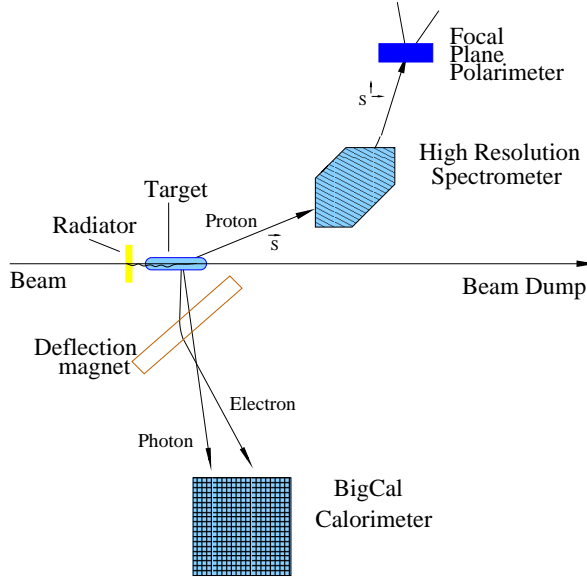


Figure 4: The experimental setup.

#### 3.1 The CEBAF Polarized Beam

Based on our experience with E99-114, we assume an incident electron beam of intensity up to  $100 \mu\text{A}$  and with 75% polarization. Such currents and polarizations have already been delivered over long periods of time using the strained GaAs source at Jefferson Lab. The beam polarization will be measured to a systematic uncertainty of 3% with the Hall A Möller polarimeter. The large cross section and helicity asymmetry for  $\pi^0$  photoproduction, as determined from E99-114, will allow a monitor of the electron beam polarization continuously during data taking at fixed kinematic conditions with large  $\theta_\gamma^{cm}$ . Continuous monitoring of the beam polarization also can be done by using the Compton polarimeter.

#### 3.2 The Liquid Hydrogen Target and the Radiator

The experiment will utilize the standard Hall A liquid hydrogen (LH2) target with a 15-cm long machined cell, which was successfully employed for many experiments in JLab.

The radiator will be mounted on the cell block about 4 inches upstream of the cell entrance window. The short distance between the target and radiator helps to avoid background produced from Al walls of the target. Even for the kinematics where the proton angle is  $6.4^\circ$ , the separation of the events produced in the radiator is 1.1 cm in the spectrometer  $y$  coordinate, which is comfortably large compared to the  $y$  resolution of 0.2 cm.

### 3.3 The Deflection Magnet

It was shown in E99-114 experiment that the deflection magnet provides sufficient separation of electron and photon elastic scattering events (see Fig. 5). The magnet obviates the need for a veto detector, which in turn allows us to utilize at least ten times higher photon intensity. The deflection magnet for the proposed experiment will be the same one constructed for and used in E99-114 (see Fig. 6). For the largest  $\theta_\gamma^{cm}=160^\circ$ , when the septum magnet should be used, the mounting and position of the deflection magnet must be changed in order to maintain sufficient out-of-plane aperture.

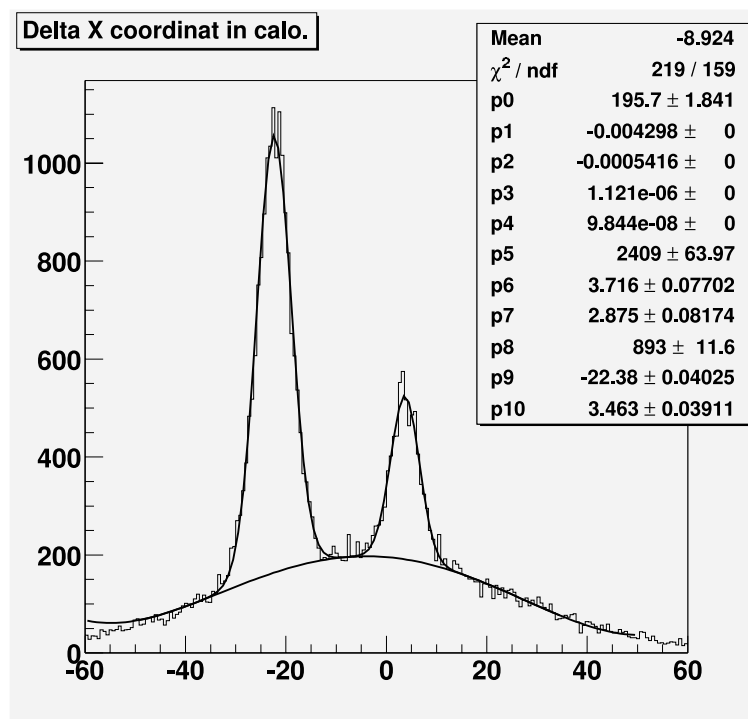


Figure 5: Experimental data from E99-114 at the kinematics  $E = 3.23 \text{ GeV}$  and  $\theta_\gamma^{cm}=98^\circ$  showing the event distribution in the horizontal plane. The peak at coordinate  $\Delta X = 0$  corresponds to the RCS events. The peak at  $\Delta X = -22$  cm corresponds to the elastic electron scattering, which is offset from the RCS peak due to the deflection magnet.

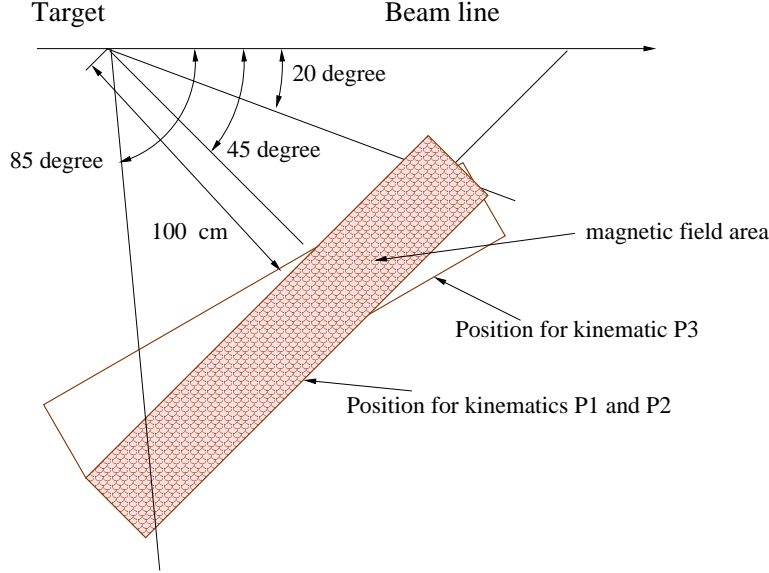


Figure 6: Layout of the deflection magnet. The magnet is indicated as the filled area as it will be used for all the measurements except for the one at  $\theta_{\gamma}^{cm} = 160^\circ$ , for which the open area will be used.

### 3.4 The Photon Calorimeter

The photon calorimeter is the main piece of instrumentation to be constructed and installed. We are participating in the construction of the BigCal calorimeter for the GEP-III experiment in Hall C [23]. This calorimeter consists of 1750 lead glass blocks of type TF-1. There are 32 columns and 56 rows of blocks. Figure 18 shows the front and top view of the calorimeter and support structure and the front end electronics. It can be moved into the hall without disconnecting the calorimeter from the front end electronics.

The position of the photon arm will be adjusted for each kinematics to match the HRS. As was successfully realized in E99-114, the movement of the calorimeter will be achieved by using the overhead crane and manual pulling of the cable train. Less than two hours (beam off to beam on) was used in a typical access into the hall for movement of the calorimeter.

### 3.5 The Data Analysis Procedure

We describe below the simplified version of the analysis procedure. The correlation between expected and observed positions of the photon on the front face of calorimeter is the primary parameter used in analysis of the RCS experiment. The expected photon position is calculated from the measured value of the proton momentum, its direction and position at the target. An example of such kinematical correlation from E99-114 is shown in Fig. 7. Three types of events are presented: RCS events, which are concentrated at the center  $\Delta X = \Delta Y = 0$ ; the photopion events, which have wider distribution in both directions  $\Delta X$  and  $\Delta Y$ ;

and the electron scattering events, which are peaked at  $\Delta X = -22$  cm,  $\Delta Y = 0$ . The events

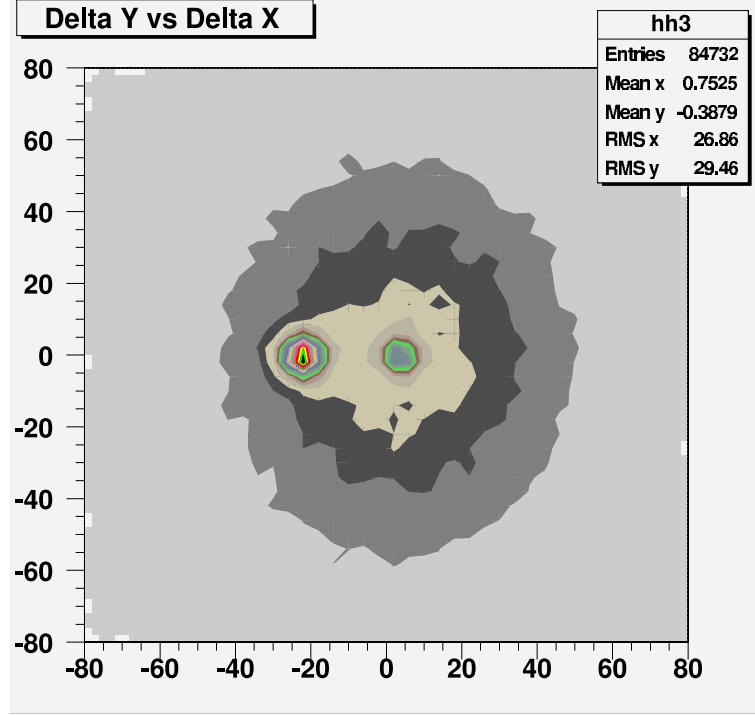


Figure 7: Experimental data from E99-114 at the kinematics  $E = 3.23$  GeV and  $\theta_{\gamma}^{cm} = 98^\circ$  showing the event distribution in the  $\Delta X - \Delta Y$  plane.

in the region of  $\pm 2\sigma$  around the Compton peak are called the correlated events. The pion event sample can be made with events located above  $\Delta Y = 2\sigma_y$  and below the  $\Delta Y = -2\sigma_y$  or with events which have  $\Delta X > 2\sigma_x$ . Figure 8 shows the  $\Delta Y$ -distribution for events with  $-2\sigma_x < \Delta X < 2\sigma_x$  when the shape of pion sample is taken from  $\Delta X > 2\sigma_x$ .

### 3.6 The Focal Plane Polarimeter

The polarization of the recoil proton is measured in the focal plane polarimeter (FPP). Figure 9 shows layout of the FPP with two analyzers, as used in E99-114. Figure 10 shows the notation of the components of the proton polarization at the target. They are  $P_l$  (longitudinal),  $P_t$  (transverse, in the reaction plane), and  $P_n$  (normal to the reaction plane). The first two are dependent on the beam helicity, whereas the last is independent. The polarization at the FPP can be found in first approximation (assuming that the HRS is a simple dipole) from expressions

$$P_t^{fpp} = P_t, \quad P_l^{fpp} = P_l \cdot \cos\chi - P_n \cdot \sin\chi$$

$$\text{and} \quad P_n^{fpp} = P_l \cdot \sin\chi + P_n \cdot \cos\chi$$



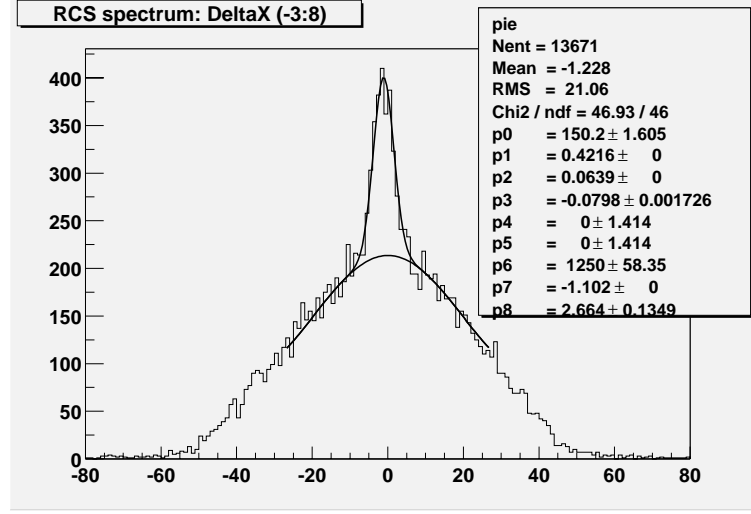


Figure 8: Experimental data from E99-114 at the kinematics  $E = 3.23 \text{ GeV}$  and  $\theta_{\gamma}^{cm} = 98^\circ$  showing the event distribution in  $\Delta Y$  for the cut  $-3 < \Delta X < 8$ .

where  $\chi$  is the spin precession angle relative to the direction of the momentum given by  $\chi = 86^\circ \cdot E_p \text{ (GeV)} [\theta_{bend}/45^\circ]$ . For example, for a proton with momentum  $3.0 \text{ GeV}/c$  the average precession angle in the HRS is  $270^\circ$ , so the longitudinal component of the proton polarization alone defines the value of the  $P_n^{fpp}$ . The  $P_n^{fpp}$  has a helicity dependent part  $P_{n,h}^{fpp}$  related to  $P_l$  and a helicity independent one related to  $P_n$ .

Figure 11 demonstrates the principles of operation of the FPP. The method is based on the scattering of the proton from the analyzer material. The number of protons which scatter from the analyzer can be expressed as a function of their polar and azimuthal angles,  $\theta$  and  $\phi$ , respectively, as

$$N^h(\phi, \theta) = N_p^h \left[ 1 + h \cdot A_y(\theta) \cdot (P_t^{fpp} \cdot \sin\phi - P_n^{fpp} \cdot \cos\phi) + A_y(\theta) \cdot (P_n^{fpp} - P_{n,h}^{fpp}) \right]$$

where  $h = \pm$  is the sign of the beam helicity;  $A_y(\theta)$  is the analyzing power, which is an empirical function of  $\theta$ , the proton momentum, and structure of the analyzer material; and the  $N_p^h$  is the total number of protons incident on the polarimeter. The FPP allows a determination of the two components of the polarization perpendicular to the proton momentum in the focal plane -  $P_t^{fpp}$  and  $P_n^{fpp}$ . Since the normal component of the proton polarization  $P_n$  is helicity-independent, all three polarization components at the target can be determined as

$$P_n = P_n^{fpp} / \cos\chi, \quad P_l = P_n^{fpp} / \sin\chi, \quad P_t = P_t^{fpp}$$

### 3.6.1 Figure-of-Merit of the Focal Plane Polarimeter

The statistical accuracy of the polarization measurement  $\delta P$  is expressed as

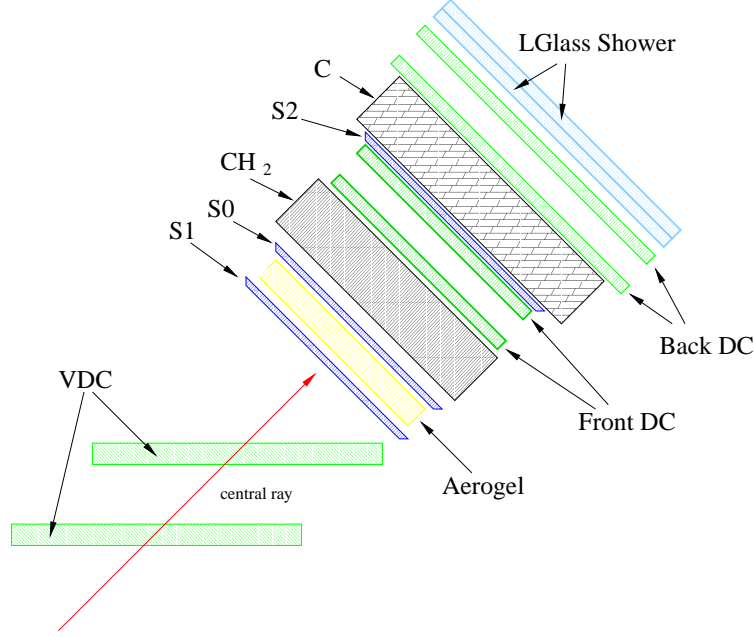


Figure 9: The structure of the detector package in the HRS with the focal plane polarimeter. The vertical drift chamber (VDC), the front drift chambers and back drift chambers are used in FPP tracking analysis. The aerogel Cherenkov counter used for pion rejection.

$$\delta P = \sqrt{2 / \left[ \epsilon A_y^2 \cdot (N_p^+ + N_p^-) \right]},$$

where  $\epsilon$  (the FPP efficiency) is the fraction of incident protons with scattering angle  $\theta$  in the range of large analyzing power;  $A_y$  is the average analyzing power over the same range of scattering angles; and  $N_p^\pm$  is the number of incident protons for each photon helicity. The Figure-of-Merit (FOM),  $\epsilon A_y^2$ , as well as total events ( $N_p^+ + N_p^-$ ), determine the statistical accuracy of the asymmetry measurement. The analyzing power depends on the proton momentum and polarimeter structure (see for example reference [24]). It is a function of the transverse component of the proton momentum after the scattering  $p_{trans} = p_p \sin\theta$ . The two most common materials used as an analyzer are Carbon and Polyethylene ( $\text{CH}_2$ ). The FOM for  $\text{CH}_2$  is 1.25 larger than that of Carbon [25]. Moreover the maximum  $A_y$  is always located at  $p_t \sim 0.30 \text{ GeV}/c$ . For optimized thickness of the analyzer, the value of the maximum was described by  $A_y = 0.40/p \text{ (GeV}/c)$  for  $\text{CH}_2$  analyzer [25].

According to the preliminary analysis of the double-analyzer FPP configuration used in E99-114, the FOM consists of 0.0013 for the  $\text{CH}_2$  (thickness = 44 cm) plus an additional 0.0006 for the Carbon analyzer (thickness = 60 cm) at  $p_p = 3.0 \text{ GeV}/c$ . These considerations lead to the total FOM of  $0.017/p_p^2 \text{ (GeV}/c)^2$ , which we use here for estimates of the required statistics and beamtime.

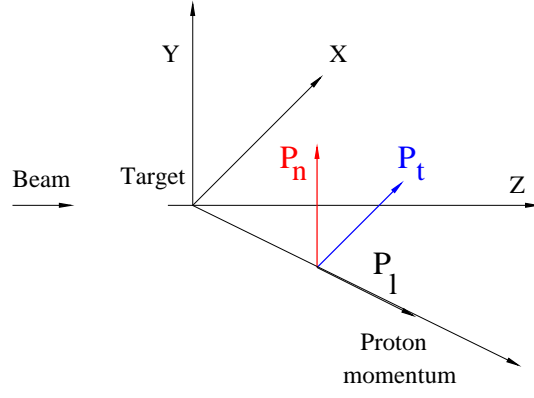


Figure 10: The definition of the polarization components at the target.

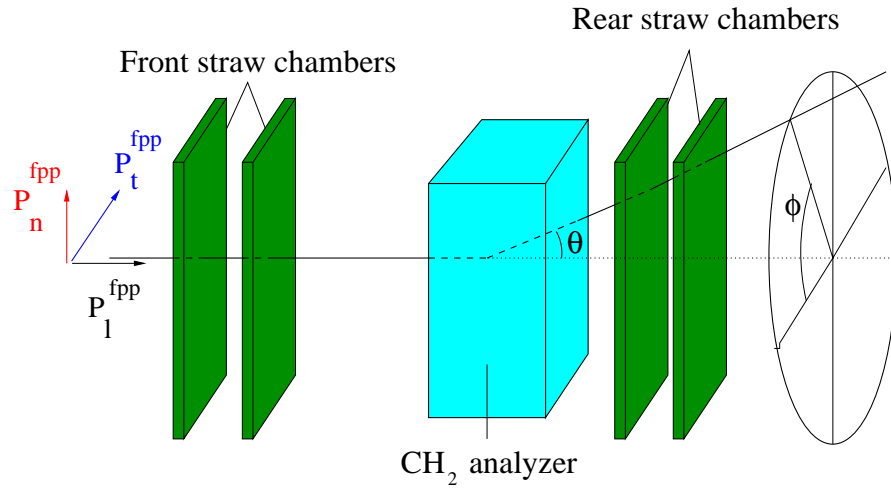


Figure 11: The operation of the Focal Plane Polarimeter.

### 3.6.2 Calibration of the Proton Polarization

Because the analyzing power is quite sensitive to the polarimeter structure, the practical way to determine the analyzing power is a calibration of the FPP using the recoil protons from elastic scattering of the polarized electrons. Calibrations allow a measure of both the analyzing power and the instrumental asymmetry. In elastic electron scattering the polarization of the recoiled proton at the target can be calculated from the following expressions [26, 27]:

$$P_{t,ep} = -\frac{2\sqrt{\tau(1+\tau)}\tan\frac{\theta}{2}}{g^2 + \tau\epsilon^{-1}} \cdot g \quad \text{and} \quad P_{l,ep} = \frac{2\sqrt{\tau(1+\tau)}\tan\frac{\theta}{2}}{g^2 + \tau\epsilon^{-1}} \cdot \frac{(E_i + E_f)\tan\frac{\theta}{2}}{2M_p}$$

where  $M_p$  is the proton mass,  $E_{i(f)}$  is the initial (final) electron energy,  $g = G_E^p/G_M^p$  is the ratio of the proton form factors,  $\tau = Q^2/4M_p^2$  with  $-Q^2 = 4E_iE_f\sin^2\frac{\theta}{2}$ , and  $\epsilon^{-1} = 1 + 2(1 + \tau)\tan^2\frac{\theta}{2}$ . The values of  $P_{t,ep}$  and  $P_{l,ep}$  determine the  $P_{t,ep}^{fpp}$  and  $P_{n,ep}^{fpp}$  used for the calibration process. The beamtime required for FPP calibration with 5% accuracy is about 10% of that RCS data-taking time.

### 3.6.3 Analysis of the Helicity Asymmetry in E99-114

E99-114 collected data with polarized photons for the average photon energy of 3.23 GeV and  $\theta_\gamma^{cm} = 122^\circ$ . Figure 12 shows the helicity asymmetry  $A_h$  observed in the distribution of recoil protons vs. azimuthal angle in the FPP for elastic electron scattering from the proton.  $A_h$  was calculated as

$$A_h(\phi) = \frac{1}{2} \left[ \frac{N^+(\phi)}{N_p^+} - \frac{N^-(\phi)}{N_p^-} \right],$$

where  $N^\pm(\phi)$  is an integral of  $N^\pm(\phi, \theta)$  over the range  $\theta = 3^\circ - 20^\circ$ . The observed asymmetries for both analyzers are about 0.053. These results were used for calibration of the FPP.

Figure 13 shows the helicity asymmetry for the  $\pi^0$  photoproduction. Figure 14 shows the asymmetry for the kinematically correlated events, where RCS and  $\pi^0$  events are mixed in ratio of 1:2. The asymmetries obtained from the above analysis are  $A_{ep}$ ,  $A_{\pi^0}$ , and  $A_{corr}$  (we dropped helicity index  $h$  in expressions here and below). Each of them has two components,  $A_t$  and  $A_n$ , denoted on the plots as  $P0$  and  $P1$ , respectively.

The asymmetry for RCS events is determined from the following:

$$A_{RCS} = A_{corr} \cdot D - A_{\pi^0} \cdot (D - 1)$$

where  $D$  is a dilution factor defined as  $(N_{\gamma,\pi^0} + N_{\gamma,\gamma})/N_{\gamma,\gamma}$  for the kinematically correlated photon-proton events. Because of the large number of  $\pi^0$  events,  $A_{\pi^0}$  is very well determined so that the accuracy of  $A_{RCS}$  is determined by the statistical precision of  $A_{corr}$ :

$$\delta A_{RCS} = D \cdot \sqrt{2/N_{corr}}$$

The  $P_t$  and  $P_n$  components of the proton polarization at the FPP for RCS are expressed as

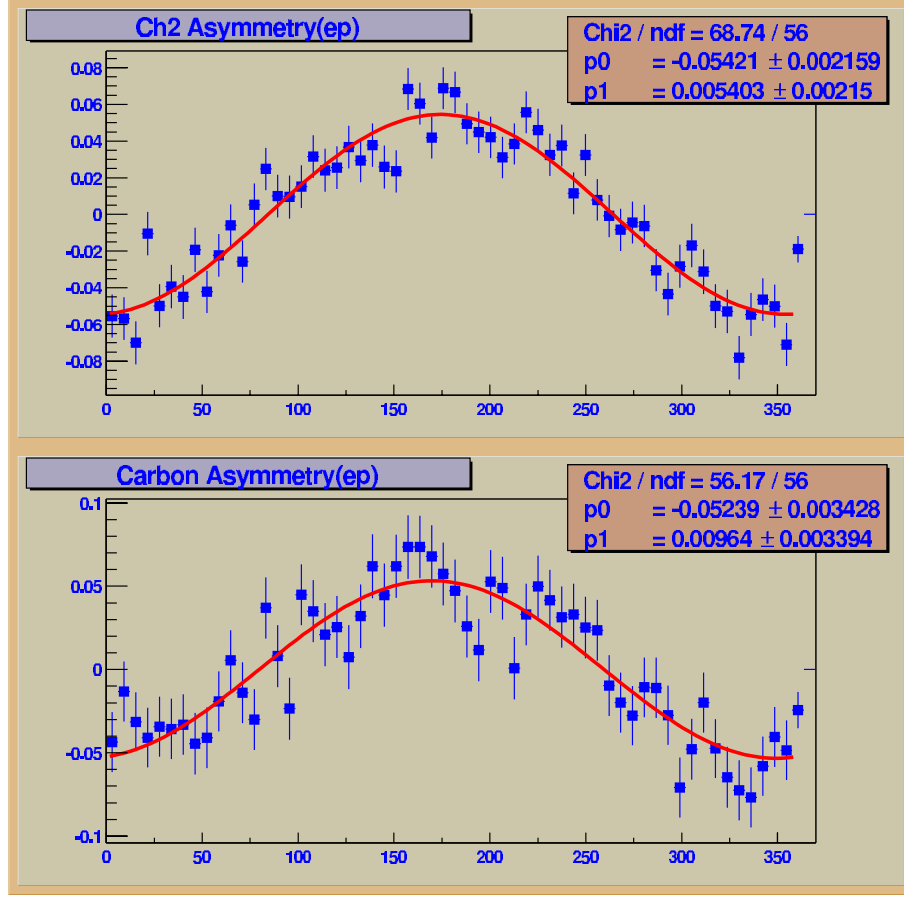


Figure 12: Beam helicity asymmetry for elastic electron scattering from proton.

$$P_{t,RCS}^{fpp} = P_{t,ep}^{fpp} \cdot [P0_{corr} \cdot D - P0_{\pi^0} \cdot (D - 1)] / P0_{ep}$$

$$P_{n,RCS}^{fpp} = P_{n,ep}^{fpp} \cdot [P1_{corr} \cdot D - P1_{\pi^0} \cdot (D - 1)] / P0_{ep}.$$

In the last formula we used the  $P0$  component of the asymmetry and  $P_{t,ep}^{fpp}$  because it is better determined than  $P1$  for the kinematics of our experiment. These formulas determine the magnitude and direction of the proton spin at the FPP in the proton rest frame relative to the direction of the proton momentum in the lab frame.

The preliminary results of E99-114 (averaged from both analyzers and normalized to 100% photon polarization) are

$$P_{l,RCS} = 0.75 \pm 0.11 \quad P_{t,RCS} = -0.10 \pm 0.10$$

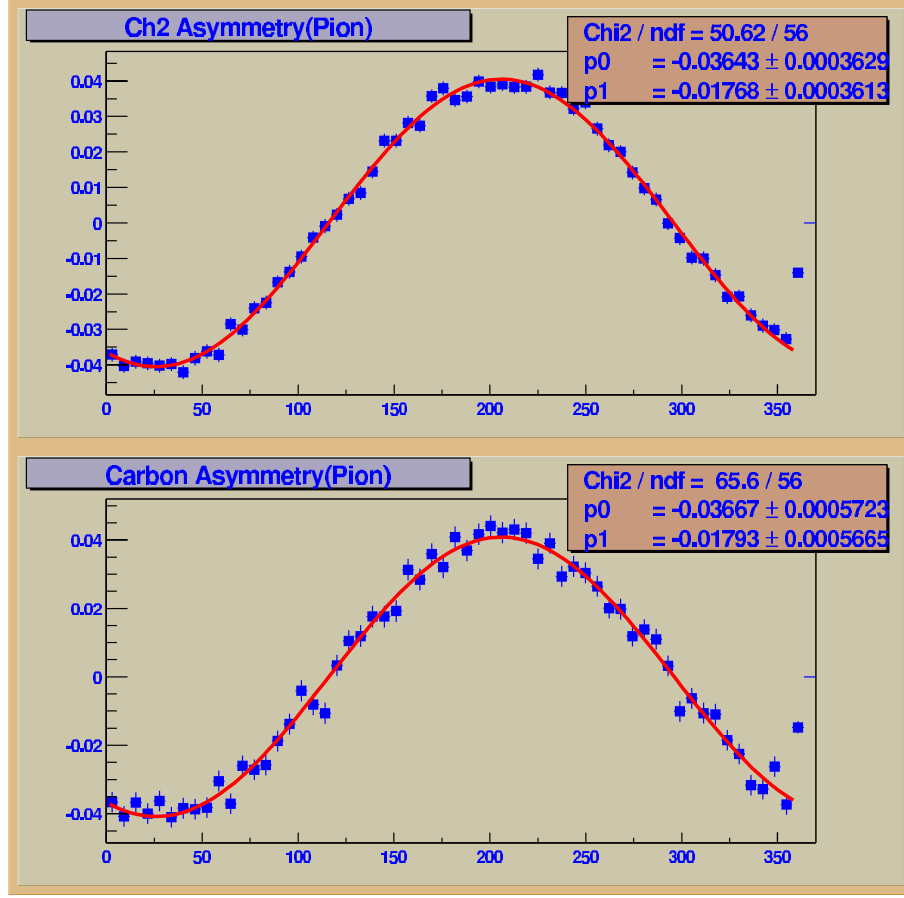


Figure 13: Beam helicity asymmetry for the  $\pi^0$  photoproduction from proton.

### 3.6.4 Transformation to the CM Frame

The FPP is calibrated based on the polarization of the proton from elastic electron scattering, whose components were calculated relative to the direction of the proton momentum in the lab frame. Therefore the results for RCS are found also relative to the direction of the the proton momentum in the lab frame. However the calculation of RCS polarization observables need to be done in photon-proton cm frame.

The transformation from lab to cm frame can be represented as a rotation of the polarization vector by angle  $\alpha$ . The magnitude of the proton polarization stays is unchanged in the transformation, but the values of the  $l$  and  $t$  components are changed as follows:

$$\begin{aligned} P_{l,RCS}^{cm} &= P_{l,RCS}^{lab} \cdot \cos\alpha - P_{t,RCS}^{lab} \cdot \sin\alpha \\ P_{t,RCS}^{cm} &= P_{l,RCS}^{lab} \cdot \sin\alpha + P_{t,RCS}^{lab} \cdot \cos\alpha \end{aligned}$$

For the kinematics of E99-114 polarization measurements,  $\alpha = 20^\circ$  which lead to polarization transfer parameters  $K_{LL} = 0.74 \pm 0.11$ ,  $K_{LT} = 0.16 \pm 0.11$ .

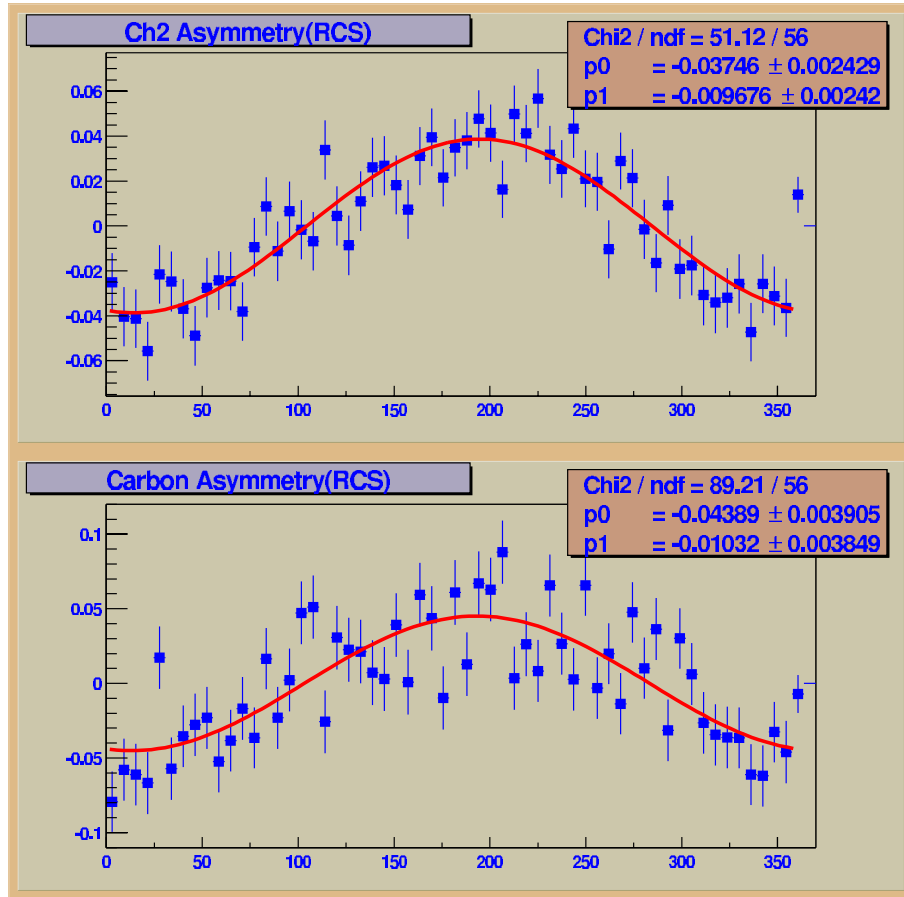


Figure 14: Beam helicity asymmetry for kinematically correlated photon-proton events.

## 4 Proposed Measurements

A longitudinally polarized electron beam with current of 100  $\mu\text{A}$  at energy of 3.5 GeV will be used. The Cu radiator with thickness of 0.8 mm (6% radiation length) will be installed 4 inches upstream of the 15 cm-long liquid hydrogen target. Photons of average energy 93% of the electron beam energy will be used. For such bremsstrahlung photons, the circular polarization is almost equal polarization of the electrons. The recoil proton will be detected in magnetic spectrometer HRS-left. The scattered photon will be detected in the large calorimeter BigCal. The components of the polarization of the recoil proton will be measured in the focal plane polarimeter (FPP). At one kinematical point the recoil proton should be detected at the lab angle  $6.4^\circ$ , which will be realized by using the septum magnet in front of the HRS. This magnet is currently under construction in Hall A for use in several experiments and will become part of the standard Hall A equipment.

All features of the experimental technique (excepting the septum magnet) were used in E99-114. The larger size of the BigCal calorimeter will allow the experiment to be done with a larger distance between the target and the calorimeter and consequently with a larger beam current by a factor of 2.5.

### 4.1 The Kinematics

The central momentum of the proton spectrometer will correspond to the elastic scattering of the photon (or electron) with initial energy 3.23 GeV (about 7% below the beam energy). The overlap of the acceptances of the photon and proton arms will be done the same way as in E99-114: The photon arm has the defining angular acceptance. Figure 15 shows the simulation of the incident photon spectra folded with the combined acceptances of the two arms. The effective photon energy range defined by the acceptance overlap is approximately 0.3-0.4 GeV. The proposed measurements are presented in Table 1, where  $\alpha$  is the spin rotation angle for transformation from the laboratory to cm frame.

kin. P #	$t$ , (GeV/c) <sup>2</sup>	$\theta_\gamma^{lab}$ , degree	$\theta_\gamma^{cm}$ , degree	$\theta_p^{lab}$ , degree	$E_\gamma^{lab}$ , GeV	$p_p$ , GeV/c	precession $\chi$ , degree	$\sin\chi$	$\alpha$ , degree
P1	1.3	23	60	48	2.53	1.33	142	0.62	36
P2	3.1	46	100	28	1.57	2.41	225	-0.71	25
P3	4.6	89	140	13	0.74	3.30	299	-0.87	17
P4	5.1	127	160	6.4	0.50	3.55	319	-0.66	16

Table 1: The kinematics parameters of the proposed measurements at  $s = 7$  (GeV/c)<sup>2</sup>.

### 4.2 Expected Rates

In E99-114 unpolarized data were collected for the average photon energy of 3.23 GeV and  $\theta_\gamma^{cm}$  in range  $75^\circ - 130^\circ$ . Table 2 presents the rate of RCS events per Coulomb of the



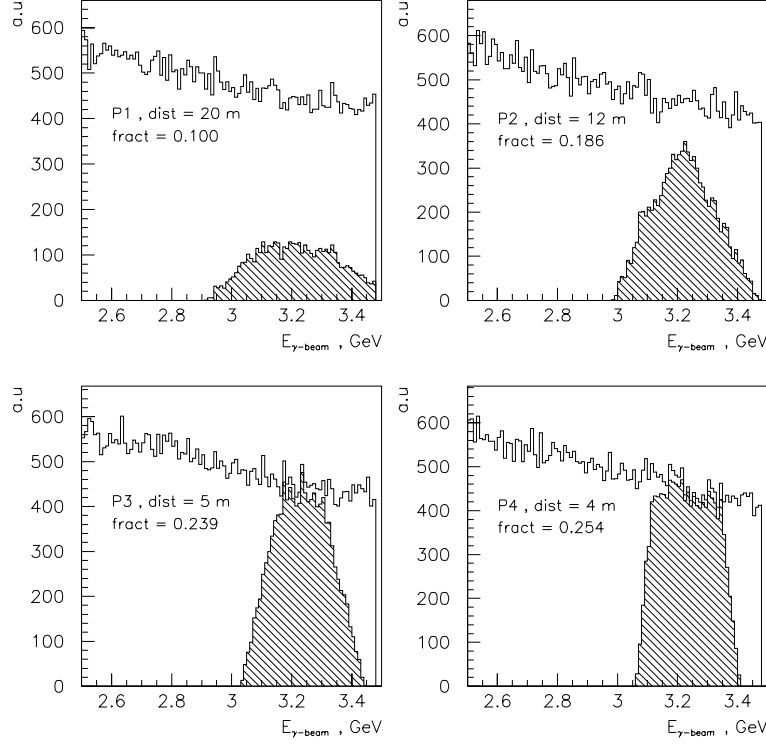


Figure 15: The simulated photon spectra for the proposed kinematics. The photon spectra in coincidence with the proton in the HRS are shown by dashed area.

beam charge for each kinematics at that photon energy. The event rates are the products of the luminosity, the cross section, and the acceptances of the detectors, as well all other factors such as DAQ dead time, efficiency of the trigger and the detectors, efficiency of the reconstruction analysis. The Table 2 also shows the dilution factor  $D$  defined as  $(N_{\gamma,\pi^0} + N_{\gamma,\gamma})/N_{\gamma,\gamma}$  for the kinematically correlated photon-proton events and the  $F_{ph.space}$ , the phase space factor for the proton arm. These observed event rates are used for an estimate of the rates in the proposed experiment. We extrapolate outside the angular region of E99-114 by noting that our preliminary analysis of the data in Table 2 shows that, within  $\pm 30\%$  systematic uncertainty, the cross section follows the expression

$$d\sigma/dt_{RCS} = d\sigma/dt_{RCS}|_{\theta_{cm}^{\gamma}=90^{\circ}} \cdot (1 - \cos\theta_{cm}^{\gamma})^{-1}$$

Table 3 presents the expected events rates per Coulomb of beam charge for the proposed measurements. For kinematics P4 we took into account the smaller solid angle of the HRS ( $4 \text{ msr} = 0.04 \cdot 0.10 \text{ rad}$ ) when it operates with the septum magnet. The distance between the target and the calorimeter was optimized to match the acceptance of the HRS, except for the limitation imposed by the 25 m radius of Hall A in case of P1 and that imposed by

kin. 3#	$\theta_\gamma^{lab}$ , degree	$\Delta\Omega_\gamma^{lab}$ , msr	$t$ , (GeV/c) <sup>2</sup>	$\theta_\gamma^{cm}$ , degree	D	$F_{ph.space}$	$N_{RCS}$ per Coulomb
3A	31	4.6	2.0	76	3.4	0.21	96,000
3B	39	9.6	2.6	89	1.8	0.21	62,000
3C	45	15.4	3.0	98	2.2	0.21	67,000
3D	57	25.0	3.7	114	2.9	0.23	81,000
3E	65	29.5	4.0	122	3.5	0.24	73,000
3F	76	34.2	4.3	131	4.3	0.24	56,600

Table 2: The rates of RCS events in the experiment E99-119.

space needed for the deflection magnet in case of P4. The resulting solid angle of the photon arm  $\Delta\Omega_\gamma^{lab}$  and acceptance factor  $F_{ph.space}$  are shown in the same table.

kin. P#	$\theta_\gamma^{lab}$ , degree	$\Delta\Omega_\gamma^{lab}$ , msr	$t$ , (GeV/c) <sup>2</sup>	$\theta_\gamma^{cm}$ , degree	D	$F_{ph.space}$	$N_{RCS}$ per Coulomb
P1	23	6.6	1.3	60	5	0.10	60,000
P2	46	18.3	3.1	100	2.3	0.19	49,000
P3	89	106.	4.6	140	5	0.24	79,000
P4	127	165.	5.1	160	6	0.25	44,000

Table 3: The expected rates of RCS events in the proposed experiment.

### 4.3 Required Statistics

As was shown in Sec. 3, the Figure-of-Merit of the FPP is approximately  $\sim 0.017/p_p^2$  (GeV/c)<sup>2</sup>. The statistics required for obtaining accuracy of  $\Delta P_l$  can be calculated

$$N_{RCS,required} = 120 \cdot p_p^2 \cdot D / \sin^2 \chi / (\Delta P_l)^2.$$

Table 4 presents required statistics for an accuracies  $\Delta P_l = 0.07$  in kinematics P1 and  $\Delta P_l = 0.10$  in P2, P3, and P4.

kinematic	P1	P2	P3	P4
$N_{RCS}$ , events	560,000	320,000	860,000	2,080,000
$\Delta K_{LL}$	0.07	0.10	0.10	0.10
$\Delta K_{LT}$	0.04	0.07	0.09	0.07
$\Delta P_N$	0.06	0.10	0.18	0.09

Table 4: The statistics and expected accuracy in the proposed experiment. The values of the error bars were not adjusted for spin rotation in the transformation between the laboratory and cm systems.

## 5 Expected Results and Beam Time Request

### 5.1 Expected Results

The purpose of this experiment is to measure the polarization transfer parameters  $K_{LL}$ ,  $K_{LT}$ , and  $P_N$  with accuracy sufficient to obtain conclusive evidence on the dominance of the specific reaction mechanism. Another purpose is to determine the form factor ratios:  $R_A/R_V$ , which is related to  $K_{LL}$ ; and  $R_T/R_V$ , which is related to  $K_{LT}/K_{LL}$ . We propose to obtain the statistical accuracies shown in Table 4, which will lead to the expected results for  $K_{LL}$  that are shown in Fig. 16. Similar statistical accuracy is expected for  $K_{LT}$  and  $P_N$ . Using the handbag formalism to interpret the results of the  $K_{LL}$  and  $K_{LT}$  measurement, we will extract values for  $R_A/R_V$  and  $R_T/R_V$  with the expected accuracy shown in Fig. 17.

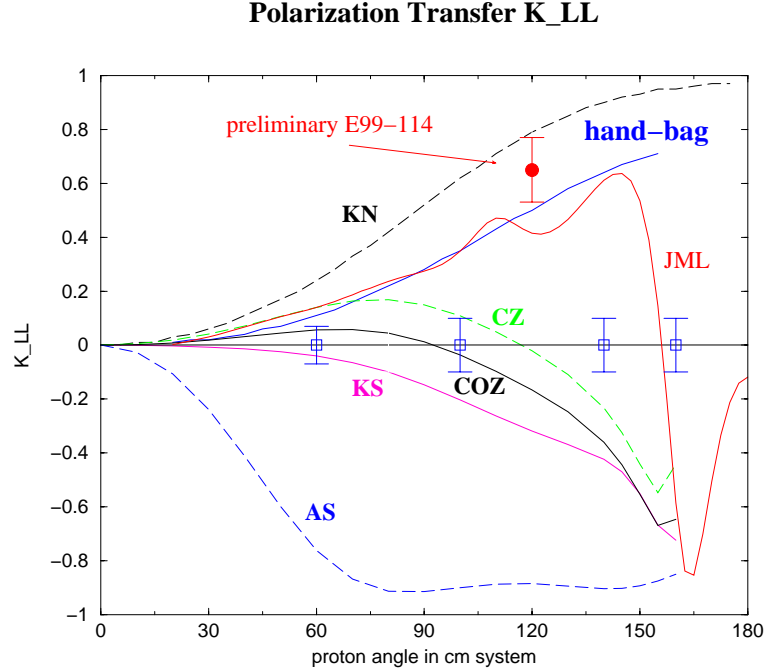


Figure 16: Polarization transfer in the RCS process with expected accuracy of the proposed measurements shown as open squares. The labels on the curves are KN for the asymmetry in the hard subprocess; the pQCD calculations [4] with AS for asymptotic distribution amplitudes, with CZ for Chernyak-Zhitnitsky [29], with COZ for Chernyak-Ogloblin-Zhitnitsky [30], with KS for King-Sachrajda [31]; hand-bag for calculations in Soft overlap approach [7], JML for calculation in Regge approach [8] .

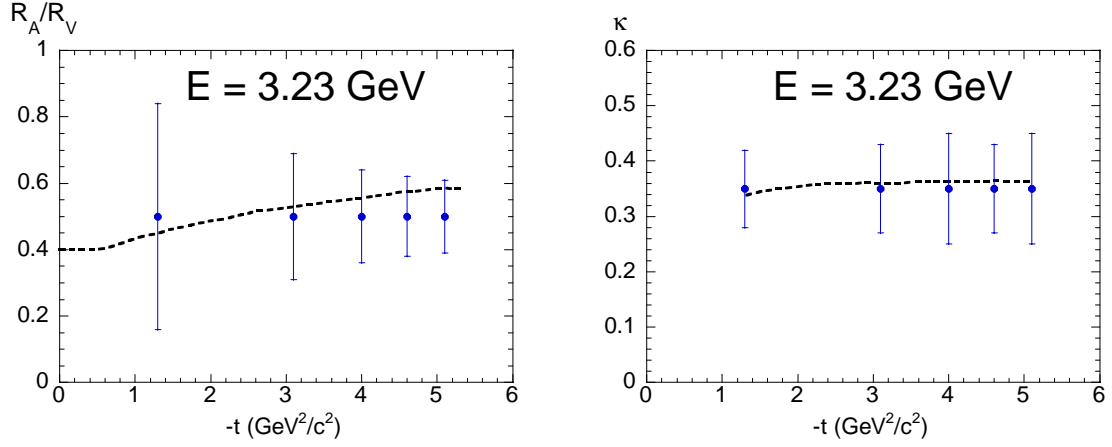


Figure 17: Expected results for the form factor ratios  $R_A/R_V$  (left) and  $\kappa$  (right). Note that  $\kappa$  is defined in Eq. 7 and is expected to be approximately constant if  $R_T/R_V$  falls as  $t^{-1/2}$ , as suggested by the results from the  $G_E^p/G_M^p$  experiment. The point at  $-t=4$   $(\text{GeV}/c)^2$  is the expected result from E99-114. The curves are predictions of Ref. [7].

## 5.2 Beam Time Request

The proposed experiment will be done at one beam energy of 3.5 GeV with current up to 100  $\mu\text{A}$ . In order to achieve the results discussed above, we require the beam time that is summarized in Tables 5 for kinematics P1-P3 and 6 for kinematics P4. The two blocks of beam times require separate setups, since the septum magnet is required for P4. A summary of the full requested beam time, 13 days, is shown in Table 7. We note that measurements at kinematics P1, P2, P3 can be done in either Hall A or Hall C. The kinematics P4 can be realized only in Hall A.

kin. P#	procedure	beam, $\mu\text{A}$	time, hours	charge Coulomb
P3	FPP calibration	100	8	3
P3	BigCal angle change		2	
P3	RCS data taking	100	31	11
P2	BigCal angle change		2	
P2	magnet shifting		6	
P2	FPP calibration	50	3	0.5
P2	RSC data taking	100	18	6.5
P1	BigCal angle change		2	
P1	FPP calibration	10	7	0.25
P1	BigCal angle change		2	
P1	RCS data taking	40	66	9.5
total			147	31

Table 5: The time allocation for kinematics P1-P3 assuming 100% efficiency.

kin. P#	procedure	beam $\mu\text{A}$	time, hours	charge Coulomb
P4	FPP calibration	100	24	9
P4	BigCal, magnet change		8	
P4	RSC data taking	100	130	47
total			162	56

Table 6: The time allocation for kinematics P4 assuming 100% efficiency.

kin. P#	beam $\mu\text{A}$	time, hours	charge Coulomb
P1-P3	10-100	147	31
P4	100	162	56
total		309	87

Table 7: The beamtime request for the experiment  
*Polarization transfer in Real Compton Scattering.*

## 6 Technical Considerations

### 6.1 The Cryotarget and Radiator

Standard Hall A cryotarget with the machined cells will be used. This cell type was used with beam current up to 100  $\mu\text{A}$  during recent experiment E01-020. The radiator will be mounted on the cell block as it was done during experiment E99-114.

### 6.2 The Calorimeter

We plan to use a calorimeter which is under construction for the experiment E01-109 [23]. Figure 18 shows the layout of the detector. It consists of 1750 blocks in 32 columns and 56 rows. The PMT FEU-83-4 will be used for light detection. This Figure also shows configuration of the calorimeter and front end electronics. The stand, which supports the calorimeter and electronics, can be moved into the hall without disassembling, so installation time need only for connecting about two thousands 100 m long cables between the detector and DAQ. Such work will require about 70 man-shifts.

GEP-III experiment plans to use trigger based on the proton arm only [28], so for RCS the trigger on the photon arm need to be constructed for use coincidence between the proton arm and the photon arm in this experiment. It will require an addition of 28 NIM fan-in-fanout modules and 7 NIM discriminators PS706.

The energy resolution for the calorimeter obtained at the beginning of the experiment E99-114 was of 5.5% (for 1 GeV photon energy) and became of 10% at the end of the run as result of radiation effects on lead glass transparency (see Fig. 19). Total accumulated beam charge in the experiment E99-114 is of 30 Coulomb. In E99-114 the front face of the lead glass was protected by plastic material with effective thickness of 10 g/cm<sup>2</sup>. Because it is found that experiment can be done without veto counters for proposed measurement we plan to use Al protection sheet of 5 cm thickness to mitigate the radiation damage of the lead glass.

We had developed and tested on the E99-114 calorimeter the technique of curing of the radiation effects. Irradiation by UV light will be done in situ without disassembling of the lead glass stock. However, it is required to remove of all PMTs, because large intensity light can damage the photocathode. Whole process of the calorimeter resolution recovery will take about 8 shifts.

### 6.3 The Proton Spectrometer

The HRS-left will be used in the proposed experiment. The trigger will be done by using S0 and S1 counters. No modification needed in the double analyzer polarimeter, which was used in experiment E99-114.

## 01-109 Calorimeter

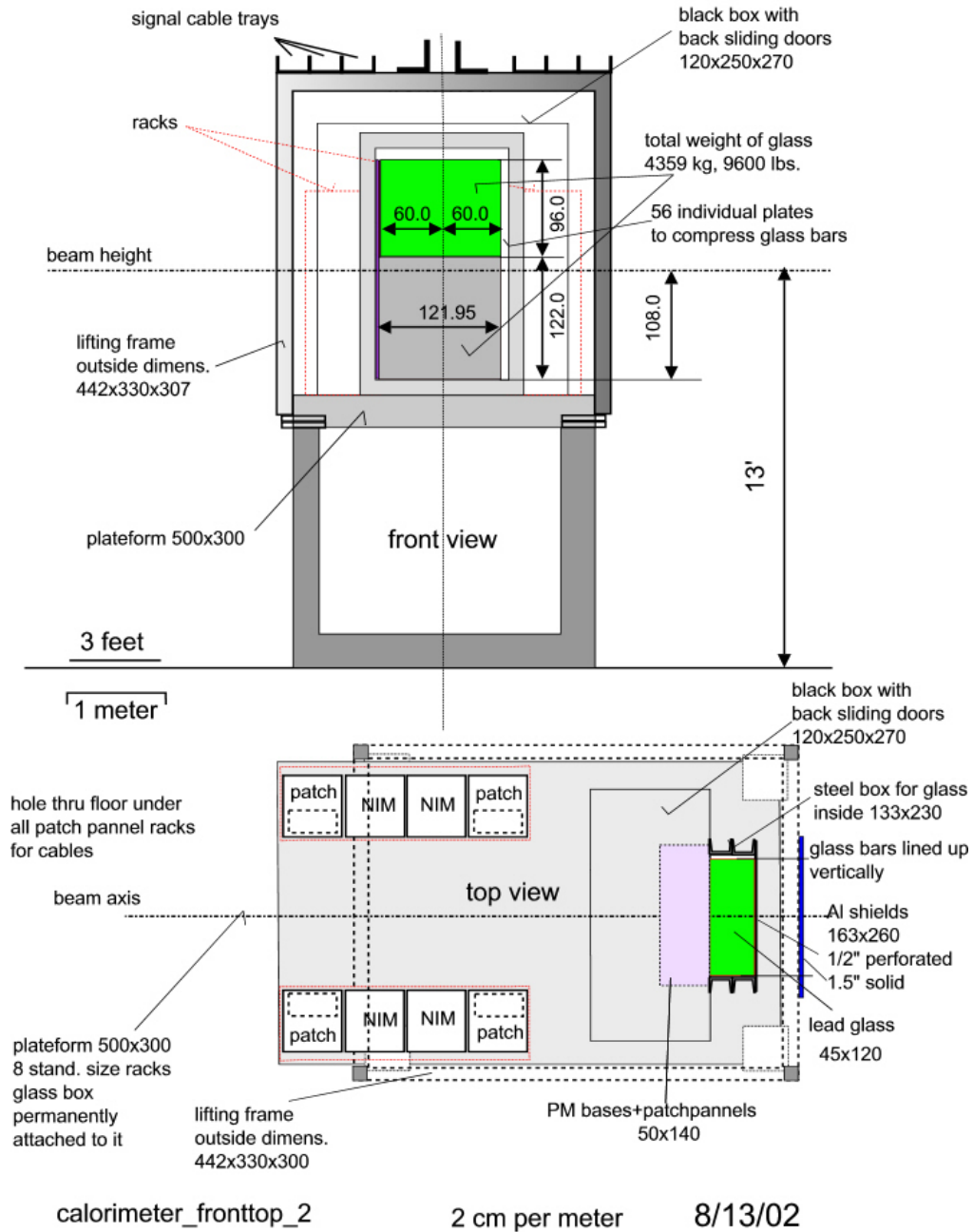


Figure 18: The structure of the BigCal calorimeter and layout of the support stand [23].

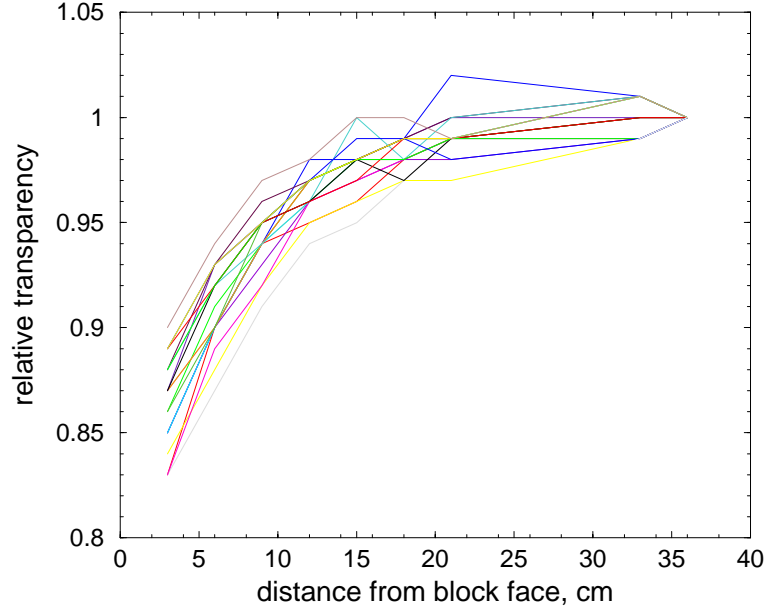


Figure 19: Transparency of lead glass blocks used in E99-114.

#### 6.4 The DAQ for the Calorimeter

The DAQ of the calorimeter, which under construction for experiment E01-109, will have almost all components required in the proposed experiment. We will need about 120 additional channels of ADC and low resolution TDC to monitor trigger signals. The coincidence logic between proton and photon arms also will be assembled. In experiment E99-114 the DAQ and HV crates of the calorimeter were located in the Hall A near the outer wall at angle of  $60^\circ$  and shielded by 10 inches of the concrete walls from the target and beam dump sides. The trip rate of the CPU was about 1-2 per shift. To mitigate the trip problem we will increase thickness of shielding by additional 10 inches or move the DAQ to the  $105^\circ$  position, where the radiation is about 15 times less, according to our calculation and measurements.



## 7 Conclusions

We request 312 hours of beamtime to measure the longitudinal and transverse components of the polarization transfer in RCS at  $s = 7 \text{ (GeV}/c)^2$  for  $\theta_\gamma^{cm} = 60, 100, 140, \text{ and } 160^\circ$ . This experiment will take place in Hall A, utilizing the polarized electron beam and HRS-left spectrometer with the focal plane polarimeter to detect protons, and BigCal calorimeter to detect scattered photons. There are no other possibility to study polarization effects in RCS.

Knowledge of the polarization transfer in RCS at these kinematics will allow a rigorous test of the reaction mechanism for exclusive reactions at high  $t$ , which is crucial for the understanding of the nucleon structure. Furthermore, it will be an extended measurement of the proton axial formfactor in RCS, which is  $1/x$  moment of the polarized parton distribution. We propose to measure polarization transfer in each kinematical point to a statistical accuracy of  $\pm 0.10$ .

## References

- [1] G. R. Farrar and H. Zhang, *Phys. Rev. Lett.* **41**, (1990) 1721, *Phys. Rev. D* **65** (1990) 3348.
- [2] A. S. Kronfeld and B. Nizic, *Phys. Rev. D* **44**, 3445 (1991).
- [3] M. Vanderhaeghen, P. A. M. Guichon and J. Van de Wiele, *Nucl. Phys. A* **622**, 144c (1997).
- [4] T. Brooks and L. Dixon, *Phys. Rev. D* **62** 114021 (2000).
- [5] A.V. Radyushkin, *Phys. Rev. D* **58**, 114008 (1998).
- [6] M. Diehl, T. Feldmann, R. Jakob, P. Kroll, *Eur. Phys. J. C* **8**, 409 (1999).
- [7] H. W. Huang, P. Kroll, T. Morii, *Eur. Phys. J. C* **23**, 301 (2002).
- [8] F. Cano and J. M. Laget, *Phys. Rev. D* **65**, 074022 (2002), hep/0209362 (accepted for publication in *Phys. Lett. B*).
- [9] C. Hyde-Wright, A. Nathan, and B. Wojtsekhowski, spokespersons, JLab experiment E99-114.
- [10] S. J. Brodsky and G. P. Lepage in *Perturbative Quantum Chromodynamics*, edited by A. Mueller (World Scientific, Singapore, 1989).
- [11] S. J. Brodsky and G. Farrar, *Phys. Rev. Lett.* **31**, 1953 (1973).
- [12] V. Matveev *et al.*, *Nuovo Cimento Lett.* **7**, 719 (1973).
- [13] S. J. Brodsky and G. P. Lepage, *Phys. Rev. D* **22**, 2157 (1980).
- [14] M. Jones *et al.*, *Phys. Rev. Lett.* **84**, 1398 (2000).
- [15] O. Gayou *et al.*, *Phys. Rev. Lett.* **88**, 092301 (2002).
- [16] K. Wijesooriya *et al.*, *Phys. Rev. C* **66**, 034614 (2002).
- [17] X. Ji, *Phys. Rev. D* **55**, 7114 (1997), *Phys. Rev. Lett.* **78**, 610 (1997).
- [18] A.V. Radyushkin, *Phys. Lett. B* **380**, 417 (1996), *Phys. Rev. D* **56**, 5524 (1997).
- [19] E. Lomon, *Phys. Rev. C* **66**, 045501 (2002).
- [20] R. L. Anderson *et al.*, *Phys. Rev. D* **14**, 679 (1976).
- [21] M. Battaglieri *et al.*, *Phys. Rev. Lett.* **87**, 172002 (2001).
- [22] T. H. Bauer, *et al.*, *Rev. Mod. Phys.* **50**, 261 (1978).

- [23] C. Perdrisat *et al.*, JLab experiment E01-109, 2001.
- [24] B. Bonin *et al.*, *Nucl. Instr. Meth.* **A 288**, 379 (1991).
- [25] I. M. Sitnik *et al.*, private communication, 2002.
- [26] A. I. Akhiezer and M. P. Rekalov, *Sov. J. Nucl. Phys.* **3**, 277 (1974).
- [27] R. Arnold, C. Carlson and F. Gross, *Phys. Rev.* **C 23**, 363 (1981).
- [28] C. Perdrisat and L. Pentchev, private communication, 2002.
- [29] V. L. Chernyak and A. R. Zhitnitsky, *Phys. Rep.* **112**, 173 (1984).
- [30] V. L. Chernyak, A. A. Oglobin, and A. R. Zhitnitsky, *Z. Phys.* **C 42**, 569 (1989).
- [31] I. D. King and C. T. Sachrajda, *Nucl. Phys.* **A 598**, 785 (1987).